AIAA JOURNAL
Vol. 32, No. 7, July 1994

Rotating Kirchhoff Method for Three-Dimensional Transonic Blade-Vortex Interaction Hover Noise

Yu Xue* and A. S. Lyrintzis†
University of Minnesota, Minneapolis, Minnesota 55455

Three-dimensional transonic blade-vortex interaction (BVI) noise is studied numerically. The unsteady transonic full-potential rotor (FPR) code is used for the simulation of the transonic BVI near-field flow. The rotating Kirchhoff method is used for the extension to the acoustic far field. Two rotating Kirchhoff formulations are developed for the three-dimensional BVI far-field noise prediction. The first formulation (Morino's method) is for an observer rotating with the blade. This allows the direct comparison with computational fluid dynamics results. The second formulation (Farassat's method) is for a stationary observer and allows a direct comparison with acoustic experiments. Test results are presented in this paper for a rotating point source and a transonic high-speed impulsive (HSI) noise prediction. The results for a parallel vortex line interacting with a nonlifting hovering rotor are presented and various cases are shown. The understanding of the three-dimensional transonic BVI noise mechanisms and directivity are discussed here.

Nomenclature

a_∞ = freestream speed of sound, 340 m/s
$\cos\theta$ = directivity parameter, $\boldsymbol{r}\cdot\boldsymbol{n}/r$
h = nondimensional time step
J = Jacobian of coordinate transformation
K = grid index of the Kirchhoff surface in the spanwise direction
k = constant for the analytical solution of a rotating point source, Eq. (18)
L = grid index of the Kirchhoff surface in the direction normal to the body
M = value of Mach number of $\boldsymbol{M}$, $|\boldsymbol{M}|$
M_t = tangential component of $\boldsymbol{M}$
$\boldsymbol{n}$ = normal unit direction of control surface, S
p = absolute pressure, N/m^2
p_∞ = freestream pressure, 101,330 N/m^2
R = radius of rotor
R_∞ = freesteam subtraction term
r = distance from observer to source, $|\boldsymbol{X}_* - \boldsymbol{X}|$
S = control surface for rotating Kirchhoff method
U = contravariant velocity in ξ direction
V = contravariant velocity in η direction
W = contravariant velocity in ζ direction
x, y, z = untransformed coordinate system
$\boldsymbol{x}$ = coordinate system fixed on the moving body
$\boldsymbol{X}$ = inertial coordinate system
Z_v = z location of the vortex line, miss distance
∇_2 = surface gradient operator
α = angle below the rotation plane, see Fig. 4
β = angle from vortex line on the rotation plane, see Fig. 4
Γ_v = nondimensional vortex strength
γ = specific heat, 1.4
ξ, η, ζ = transformed coordinate system
$\hat{\theta}$ = transmission time, $t_* - \tau$
Φ = velocity potential
ψ = rotor azimuthal angle, deg
ρ = fluid density normalized by freestream values
$\hat{\rho}$ = ρ/J
ω = angular velocity of S

Subscripts

v = vortex
∞ = conditions at infinity
$*$ = observer location

Received June 14, 1993; revision received Jan. 28, 1994; accepted for publication Feb. 10, 1994.

*Graduate Student; currently Aerospace Engineer, ART Inc., 1685 Plymouth Street, Mountain View, CA 94043. Member AIAA.

†Assistant Professor, Aerospace Engineering and Mechanics. Member AIAA.

Introduction

In recent years the increasing use of helicopter and the projected use of tilt-rotor aircraft have drawn attention to the noise that they generate. Among the several types of helicopter and tilt rotor aircraft noise, that due to blade-vortex interactions (BVI) is one of the most important. A numerical study of this phenomenon has been made in the past using a small disturbance, two-dimensional unsteady transonic flow code (VTRAN2).[1–4] In Refs. 5–11, the two-dimensional transonic BVI problem is solved using the small disturbance theory and the more complex Euler and thin-layer Navier Stokes equations. A new look at the physics of the noise mechanisms of unsteady transonic flow is given by Lyrintzis and Xue[12] and Lyrintzis et al.,[13] who propose a correlation between lift and drag forces and the acoustic disturbances. Baeder et al.[14] present some near- and midfield results. A direct comparison of the flow results obtained from the different methods (from small disturbance to Navier Stokes equations) shows that the results are very similar (e.g., Ref. 15). In fact, the results tend to coincide at greater distances from the airfoil surface. However, at great distances from the airfoil, the waves become very difficult to follow because of numerical diffusion and dispersion errors. Thus, to study the far field a more accurate method is needed.

In the past both a full flowfield solution (e.g., Ref. 16) and the acoustic analogy (e.g., Ref. 17) have been used in rotorcraft aeroacoustics. However, a full flowfield solution is very expensive because it needs very fine grid to get accurate far-field results. For the acoustic analogy it should be noted that there are substantial difficulties in including the nonlinear quadrupole term (which requires second derivatives) in the volume integrals, especially around moving shock surfaces. Thus, many investigators use near-field data only on the blade surface (e.g., Refs. 18 and 19), a method which is less accurate in the transonic cases since the effects of moving shocks and compressibility in the near field are not accounted for.

An innovative approach called the Kirchhoff method has been successfully used to extend the numerical nonlinear aerodynamic

near-field results to the linear acoustic far field. The full nonlinear equations are solved in the first region (near field) numerically, and a surface integral of the solution over the control surface gives enough information for the analytical calculation in the second region (far field). An advantage of the Kirchhoff method is that the surface integrals and the first derivatives needed can be easily evaluated from the near-field numerical aerodynamic data; full diffraction and focusing effects are included nevertheless eliminating the propagation of the reactive near field. The method is simple and accurate, as it especially accounts for the shock-related noise in the far field. A recent review of the uses of Kirchhoff's method in aeroacoustics can be found in Ref. 20. The method was first applied in helicopter acoustics for the calculation of two-dimensional transonic BVI noise with very good results.[2-4]

For three-dimensional applications, Baeder et al.[21] and Strawn et al.[22] used a stationary Kirchhoff surface that encloses the entire rotor. The state-of-the-art transonic unsteady rotor Navier Stokes (TURNS) code[22,23] was used for the near-field computational fluid dynamics (CFD) calculations. An unstructured grid was used by Strawn et al.[24] The method predicted the high-speed impulsive (HSI) hover noise very well using about half the CPU of the straight CFD calculation. The results are also compared with acoustic analogy. The acoustic analogy results were inaccurate for tip Mach numbers higher than 0.7. It should be noted that detailed CFD information out to the stationary Kirchhoff cylinder is necessary as an input. In addition, the aerodynamic input, which is usually in rotating blade coordinates, has to be transformed to stationary coordinates, a process that introduces some errors.

For BVI, all previously published results for the numerical computation of the acoustics of transonic BVIs are limited to two dimensions. However, it is very hard to compare the two-dimensional numerical results to the results from three-dimensional experiments and actual in-flight tests. Thus, a three-dimensional model utilizing the full potential rotor (FPR) code with a rotating Kirchhoff method for obtaining far-field noise is developed here for the first time. A rotating Kirchhoff formulation allows the Kirchhoff surface to rotate with the blade; thus, a smaller cylinder surface around the blade can be used. No transformation of data is needed since the CFD are also rotating. Since a more detailed information is utilized for the accurate prediction of the far-field noise, this method is more efficient. We feel that the rotating Kirchhoff formulation is necessary for the BVI problem, since the details of the flow around the airfoil caused by the vortex are important for the far-field noise.

This paper will demonstrate that the rotating Kirchhoff formulation coupled with the FPR code is able to predict three-dimensional transonic BVI far-field noise as well as high-speed impulsive noise and could lead to a better understanding of the BVI noise mechanisms and directivity. A version of this work was given in Ref. 25. The parallel BVI model used in study is based on Caradonna's wind-tunnel experiment configuration.[26] However, the parallel BVI is shown to be very similar to those produced by the rotor alone while operating in a normal descent mode.[26]

Full-Potential Rotor Code

The full-potential rotor code[26,27] uses finite difference schemes, which compute three-dimensional transonic flows around rotor blades. It is fast compared with Euler and Navier Stokes equations solutions and still gives a realistic representation of the physical flowfield. Major assumptions for a full-potential model are that the flowfield is both inviscid and irrotational. For a transonic rotor, neither of these assumptions is violated. The flowfield is dominated by inviscid effects, and the shocks are not strong enough to generate sizable vorticity. The near-field results from the FPR should provide accurate information for far-field calculation by using the rotating Kirchhoff method. Figure 1 shows the physical model of the three-dimensional parallel BVI, which is based on Caradonna's wind-tunnel experiment configuration.[26]

The FPR code solves the three-dimensional, unsteady transonic full-potential equation in strong conservation form. This equation is written in generalized coordinates

$$\frac{\partial}{\partial\tau}\left(\frac{\rho}{J}\right)+\frac{\partial}{\partial\xi}\left(\frac{\rho U}{J}\right)+\frac{\partial}{\partial\eta}\left(\frac{\rho V}{J}\right)+\frac{\partial}{\partial\zeta}\left(\frac{\rho W}{J}\right)=0 \tag{1}$$

with density given by

$$\rho=\left\{1-\frac{\gamma-1}{2}[2\Phi_\tau+(U+\xi_t)\Phi_\xi+(V+n_t)\Phi_\eta+(W+\zeta_t)\Phi_\zeta]\right\}^{1/(\gamma-1)} \tag{2}$$

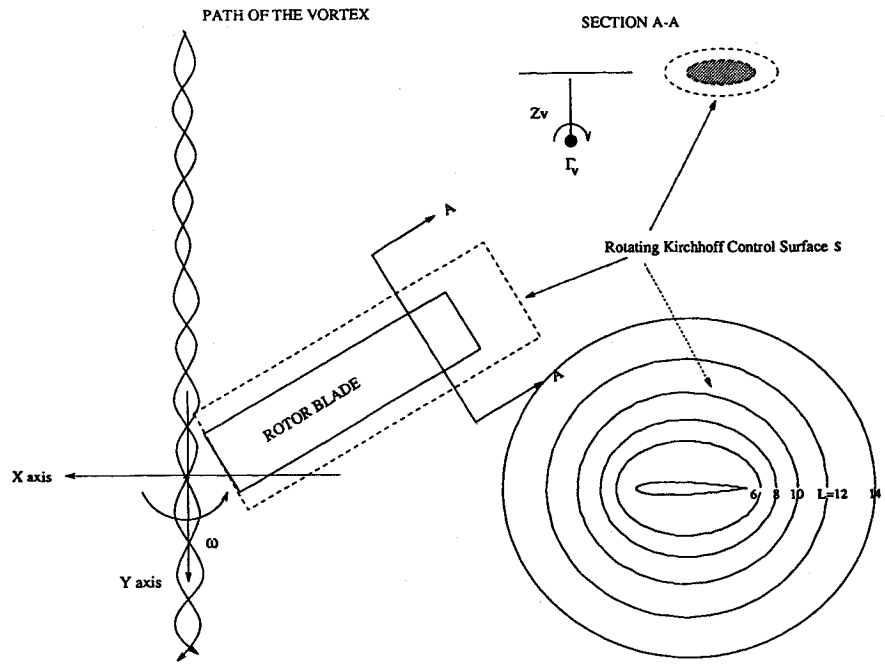

Fig. 1 Hover parallel blade-vortex interaction and rotating Kirchoff surface *S*.

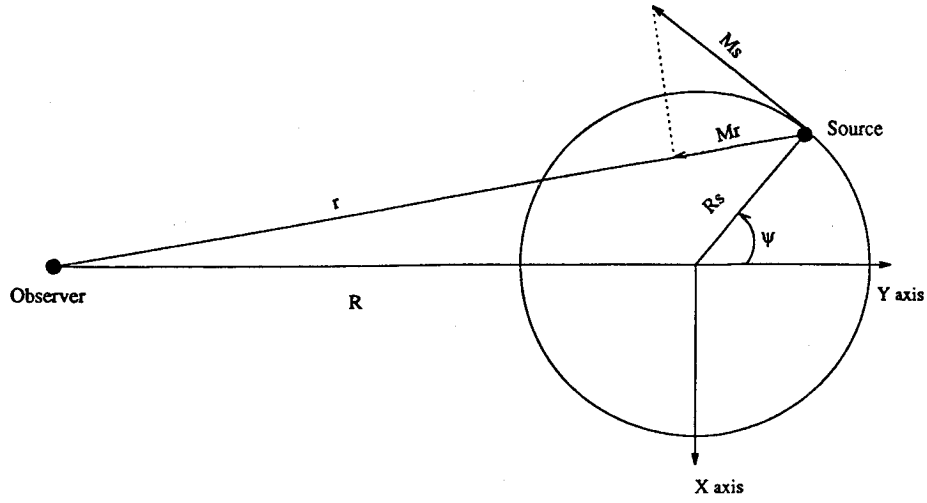

Fig. 2 Rotating constant point source and an observer.

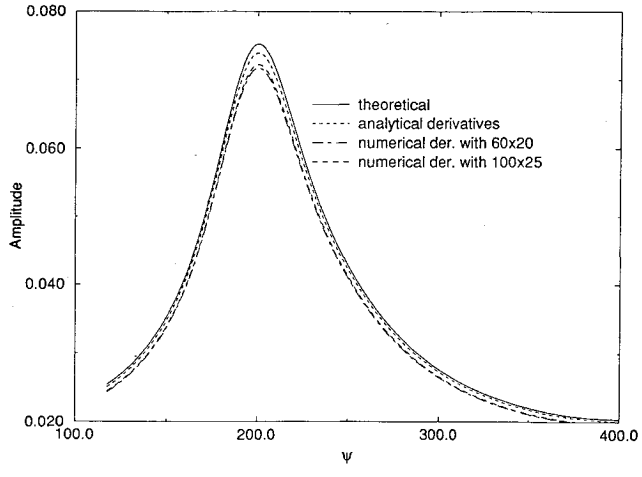

Fig. 3 Comparison between a theoretical and numerical solution for the rotating constant point source, *Ms* = 0.5, at position *R* = 3 *Rs* (*Rs* is the source radius).

where U, V, and W are contravariant velocities along the ξ, η, and ζ directions, respectively, given by

$$\begin{aligned} U &= \xi_t + A_1\Phi_\xi + A_4\Phi_\eta + A_5\Phi_\zeta \\ V &= \eta_t + A_4\Phi_\xi + A_2\Phi_\eta + A_6\Phi_\zeta \\ W &= \zeta_t + A_5\Phi_\xi + A_6\Phi_\eta + A_3\Phi_\zeta \end{aligned} \tag{3}$$

and

$$\begin{aligned} A_1 &= \xi_x^2 + \xi_y^2 + \xi_z^2 \\ A_2 &= \eta_x^2 + \eta_y^2 + \eta_z^2 \\ A_3 &= \zeta_x^2 + \zeta_y^2 + \zeta_z^2 \\ A_4 &= \xi_x\eta_x + \xi_y\eta_y + \xi_z\eta_z \\ A_5 &= \xi_x\zeta_x + \xi_y\zeta_y + \xi_z\zeta_z \\ A_6 &= \eta_x\zeta_x + \eta_y\zeta_y + \eta_z\zeta_z \end{aligned} \tag{4}$$

$$J = \xi_x(\eta_y\zeta_z - \eta_z\zeta_y) + \eta_x(\xi_z\zeta_y - \xi_y\zeta_z) + \zeta_x(\xi_y\eta_z - \xi_z\eta_y) \tag{5}$$

$A_1 - A_6$ are metric quantities, and J is the Jacobian of the transformation $|\partial(\xi, \eta, \zeta)/\partial(x, y, z)|$.

All velocities are normalized by a_∞, distances by the airfoil chord length c, and time by the combination (c/a_∞). Density is normalized by the freestream value ρ_∞. The resulting equation is approximately factored into L_ξ, L_η, and L_ζ operators.

$$\begin{aligned} L_\xi L_\eta L_\zeta(\Phi^{n+1} - \Phi^n) &= (h^2/\hat{\beta}^n)[\delta_\xi(\hat{\rho}U)^n + \delta_\eta(\hat{\rho}V)^n \\ &+ \delta_\zeta(\hat{\rho}W)^n - R_\infty] + C \end{aligned} \tag{6}$$

where

$$\begin{aligned} L_\xi &= [I + hU^n\delta_\xi - (h^2/\hat{\beta}^n)\delta_\xi(\hat{\rho}A_1)^n\delta_\xi] \\ L_\eta &= [I + hV^n\delta_\eta - (h^2/\hat{\beta}^n)\delta_\eta(\hat{\rho}A_2)^n\delta_\eta] \\ L_\zeta &= [I + hW^n\delta_\zeta - (h^2/\hat{\beta}^n)\delta_\zeta(\hat{\rho}A_3)^n\delta_\zeta] \end{aligned} \tag{7}$$

and where δ_ξ, δ_η, and δ_ζ represent central difference operators in space, and the term C is

$$\begin{aligned} C = [I + h(\hat{\beta}^{n-1}/\hat{\beta}^n)(U^{n-1}\delta_\xi + V^{n-1}\delta_\eta + W^{n-1}\delta_\zeta)](\Phi^n - \Phi^{n-1}) \\ + (\hat{\beta}^{n-1}/\hat{\beta}^n)(\Phi^n - 2\Phi^{n-1} + \Phi^{n-2}) + (h/\hat{\beta}^n)(\hat{\rho}^n - \hat{\rho}^{n-1}) \end{aligned} \tag{8}$$

The bracketed term in Eq. (8) represents the temporal conservation correction to the algorithm. In Eqs. (6–8), h is the time step, $\hat{\beta} = \rho^{2-\gamma}/J$, and $\hat{\rho} = \rho/J$. The superscript n represents the time step.

The pressure disturbance can be obtained by using the following equation:

$$p = (\rho^\gamma - 1)p_\infty \tag{9}$$

A steady-state alternating direction implicit (ADI) relaxation algorithm can be obtained from Eq. (6) by omitting the unsteady C term on the right-hand side of the equation. The steady-state solution coupling with the rotating Kirchhoff method will be able to predict the far-field acoustic solution for high-speed impulsive noise, which will be discussed later.

On the surface of a blade a flow tangency condition is chosen. At the outer radial boundary of the grid, a nonreflective boundary condition is used to prevent the accumulation of numerical disturbances. A spanwise series of body-fitted parallel O grids are used for the basic grid system. Rotor flows are computed by assigning

an appropriate rotational coordinate velocity to each grid point. Upwind biasing of the density is used in regions of supersonic flow to stabilize the solution. A prescribed vortex velocity field (i.e., transpiration method) is specified in the FPR code using a velocity decomposition method as it is used in Ref. 26. The total velocity field is written as the sum of a gradient of the potential and a known velocity field created by the vortex. Half-point differencing formulas have been implemented for both density and metric calculations, which improves the accuracy and robustness of the code. Further details can be found in Refs. 26 and 27.

It should be noted here that the Bernoulli equation for density is only valid for isentropic, irrotational flow. Thus, it will cause some inaccuracy in the occurrence of a strong shock wave as well as in the calculation within the rotational vortex core. However, this problem has not been significant for the BVI cases investigated in this paper.

Far-Field Acoustic Formulation

In our approach, a rigid control surface S warped around the rotating blade (Fig. 1) is used. The linear acoustics approximation for pressure is assumed outside of this control surface whereas the inside of the control surface is the unsteady transonic flowfield. The near-field flow solution is computed by FPR code; then the far-field acoustic signal at one observer's position is computed by a surface integral representation on the closed control surface S, where evaluations on the surface are provided from the known near-field flow solution. Since the control surface is rotating with the blade, this surface integration has to be presented by one of following stated rotating Kirchhoff formulations and this technique is referred as the rotating Kirchhoff method.

Theoretical Background

The three-dimensional rotating Kirchhoff formula uses a Green's function for the linearized governing equation to derive a representation for the solution in terms of its values and derivatives on a closed surface in space, which is assumed to include all of the nonlinear effects.[20] In the case that the blade is in uniform rotation (three-dimensional BVI), a rotating Kirchhoff control surface S, as well as the corresponding rotating Kirchhoff formulation, are employed herein.

Since the rotating Kirchhoff method assumes that linear equations are valid outside the closed rotating control surface S, S must be chosen large enough to include the region of all nonlinear behavior. However, the accuracy of the numerical solution is limited to the region immediately surrounding the moving blade because of the increase in mesh spacing with distance in the FPR code. Thus, a judicious choice of S is required for the effectiveness of the Kirchhoff method. Surfaces S from $L = 6$ to $L = 14$ are chosen (based on our experience from numerical experiments), where L is the grid index in the direction normal to the body shown in Fig. 1. Higher Mach numbers require larger surfaces because the persistence in the nonlinear regions are larger. It should be mentioned here that a closed Kirchhoff control surface S shown in Fig. 1 consists of three surfaces: one is a cylinder-like surface warped around the rotating blade, the other two surfaces are the surfaces on the top and bottom of the cylindrical surface. However, the effect from the bottom surface on root of blade is insignificant; only the cylindrical surface and top surface are considered in our cases here.

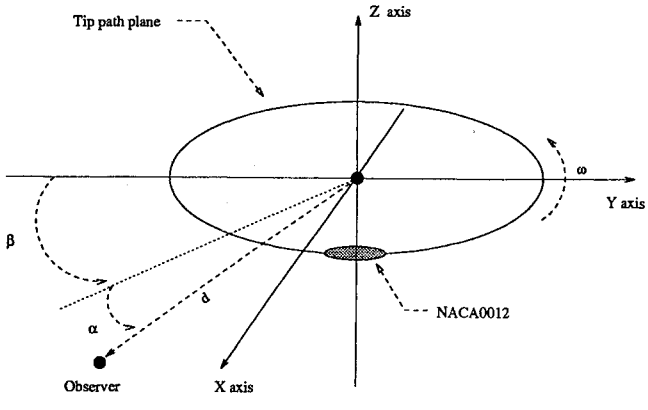

Fig. 4 Observer's position for a rotating blade.

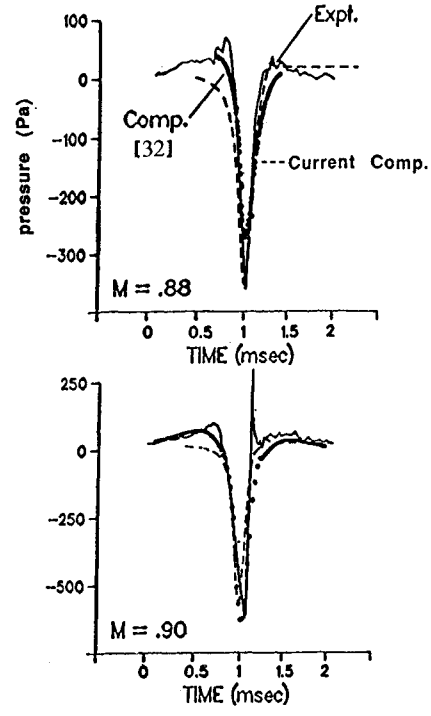

Fig. 5 HSI acoustic pressure predictions for two hover tip Mach numbers, $M = 0.88$ and 0.9 at position $d = 3R$, $\alpha = 0$ deg, $\beta = -22.3$ deg; experiments and computations from Ref. 32 are also shown.

The first method of obtaining a rotating Kirchhoff formula is to adapt the formula derived by Morino and Tseng[28] (i.e., Morino's formula). This formula was originally derived to calculate the aerodynamics of potential flow around a helicopter blade. For the purposes of acoustic calculations, the nonlinear term in Morino's formula is neglected, and the surface integration is applied on the rotating Kirchhoff control surface S (see Fig. 1) instead of on the surface of blade used in Morino's formula.

Morino's rotating Kirchhoff formulation gives the pressure signal of an observer in the rotating coordinate system as a function of the surface integral over control surface S of the pressure, the normal derivative of the pressure, and the time derivative of the pressure, which can be obtained from solutions of a near-field solver such as the FPR code

$$p(\boldsymbol{x}_*, t_*) = \frac{1}{4\pi}\iint_S \left[\frac{-1}{\hat{\rho}}\frac{\partial p}{\partial n} - \frac{\partial}{\partial \hat{n}}\left(\frac{-1}{\hat{\rho}}\right)p + \frac{-1}{\hat{\rho}}\frac{\partial p}{\partial t}\left(\frac{\partial \theta}{\partial \hat{n}} + 2\frac{\boldsymbol{M}\cdot\boldsymbol{n}}{a_\infty}\right)\right]_{\tau^*} \mathrm{d}S \tag{10}$$

where

$$\frac{\partial}{\partial \hat{n}} = \frac{\partial}{\partial n} - \boldsymbol{M}\cdot\boldsymbol{n}\boldsymbol{M}\cdot\nabla_x, \qquad \frac{\partial}{\partial \hat{n}} = -\boldsymbol{n}\cdot\nabla_{x_*} + \boldsymbol{M}\cdot\boldsymbol{n}\boldsymbol{M}_*\cdot\nabla_{x_*} \tag{11}$$

Equations (10) and (11) are valid for any arbitrarily moving surface. For the case of a rotoring surface (hover),

$$\boldsymbol{M} = \frac{1}{a_\infty}(\boldsymbol{\omega}\times\boldsymbol{X}), \quad \boldsymbol{M}_* = \frac{1}{a_\infty}(\boldsymbol{\omega}\times\boldsymbol{X}_*), \quad \hat{\rho} = r(1 - M_r) \tag{12}$$

Here the location with the asterisk represents the observer's location, and the location without the asterisk represents the source's

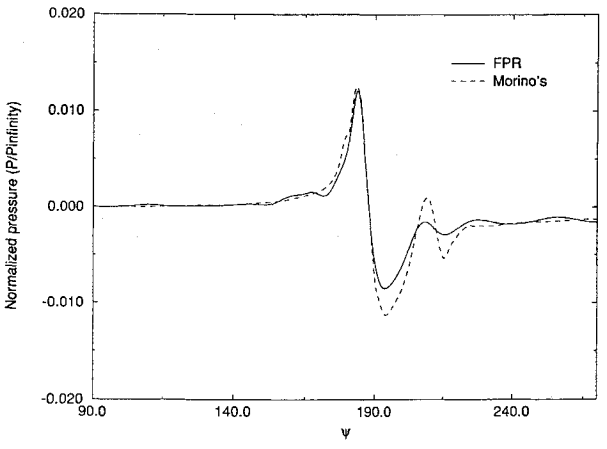

Fig. 6 Acoustic pressure prediction using Morino's method for hover parallel BVI, $M = 0.75$, $\Gamma_v = 0.2$, $Z_v = -0.26$ at position $x_* = -0.56$, $y_* = 9.89$, $z_* = 0.705$ on $L = 11$.

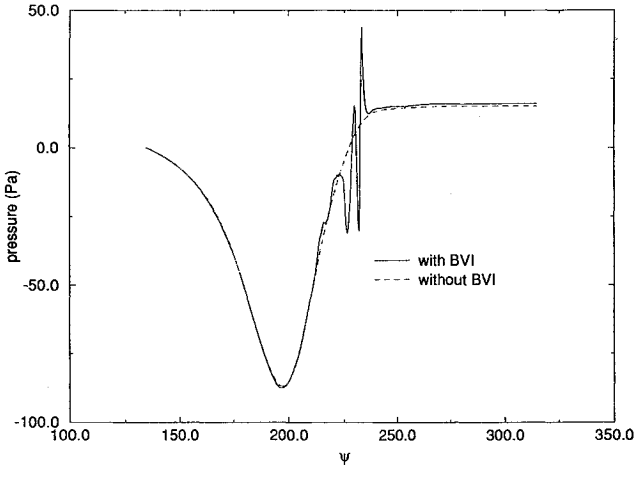

Fig. 7 Acoustic pressure predictions by using Farassat's method for hover parallel BVI, $M = 0.75$, $\Gamma_v = -0.2$, $Z_v = -0.26$ at position $d = 3R$, $\alpha = 0$, $\beta = 0$.

position. The τ^* is the source emission time (or retarded time) and is the solution of equation

$$\tau - t_* + |X_*(t_*) - X(\tau)|/a_\infty = 0 \tag{13}$$

where τ denotes the source time and t_* the observer time, and $\theta = \tau^* - t_*$ (used in Eq. 10). All quantities in the integral of Eq. (10) are evaluated in the source emission time. $\boldsymbol{M}$ and $\boldsymbol{n}$ are the speed Mach number and normal direction unit of the rotating Kirchhoff control surface S, respectively.

The retarded time Eq. (13) can be solved numerically using a Newton-Raphson technique. When the surface S moves subsonically, Eq. (13) has a unique solution. Only subsonically moving surfaces are examined here. It should be noted that the observer in this formula is moving with the source, and so it is almost impossible to get this kind of experimental far-field results for comparison. The advantage of this method though is that the results can be compared with CFD results (i.e., from FPR) for the position not too far from the blade but outside of the Kirchhoff control surface S.

The second method of obtaining the rotating Kirchhoff formula is to use a formula given by Farassat and Myers.[29] In this formulation the observer is stationary whereas the Kirchhoff control surface is in rotation, so it is possible to get experimental results that can be compared with our calculations. For this reason, Farassat's formula has been primarily used in this paper. For both methods, we have assumed that the rotating Kirchhoff control surface S is rigid for the simplicity.

Farassat's rotating Kirchhoff formulation gives the pressure signal of an observer in the stationary coordinate system as a function of the surface integral over the control surface S of the pressure, the normal derivative of the pressure, and the time derivative of the pressure

$$p(\boldsymbol{X}_*, t_*) = \frac{1}{4\pi}\iint_S \left[\frac{E_1}{r(1-M_r)} + \frac{E_2 p}{r^2(1-M_r)}\right]_{\tau^*} \mathrm{d}S \tag{14}$$

where

$$E_1 = (M_n^2 - 1)\, p_n + M_n \boldsymbol{M}_t \cdot \nabla_2 p - a_\infty^{-1} M_n \dot{p}$$

$$+ \frac{a_\infty^{-1}}{(1-M_r)}\left[(\dot{n}_r - \dot{M}_n - \dot{n}_M)\, p + (\cos\theta - M_n)\dot{p}\right]$$

$$+ \frac{a_\infty^{-1}}{(1-M_r)^2}\left[\dot{M}_r(\cos\theta - M_n)\, p\right] \tag{15}$$

$$E_2 = \frac{1-M^2}{(1-M_r)^2}(\cos\theta - M_n)$$

$\boldsymbol{M}$ and $\boldsymbol{n}$ have the same amplitude as in Morino's formulation but have to be multiplied by the rotating coordinate transformation matrix for the directions. Here the dots over $\boldsymbol{M}$ and $\boldsymbol{n}$ denote the source emission time τ^* derivative. The τ^* is the source emission time and is the solution of the equation

$$\tau - t_* + |X_* - X(\tau)|/a_\infty = 0 \tag{16}$$

In addition, the following definitions are introduced:

$$\dot{M}_r = \dot{\boldsymbol{M}} \cdot \hat{\boldsymbol{r}}, \qquad \dot{n}_r = \dot{\boldsymbol{n}} \cdot \hat{\boldsymbol{r}}, \qquad \dot{M}_n = \dot{\boldsymbol{M}} \cdot \boldsymbol{n}$$

$$\dot{n}_M = \dot{\boldsymbol{n}} \cdot \boldsymbol{M}, \qquad \dot{\boldsymbol{n}} = \omega \times \boldsymbol{n} \tag{17}$$

It should be noted that the simplified expression in Eq. (15) for E_2 was given by Myers and Hausmann,[30] whereas in the original paper of Farassat and Myers,[29] a more complicated formula was presented.

It should be mentioned that Morino's formula and Farassat's formula should be mathematically equivalent after a coordinate

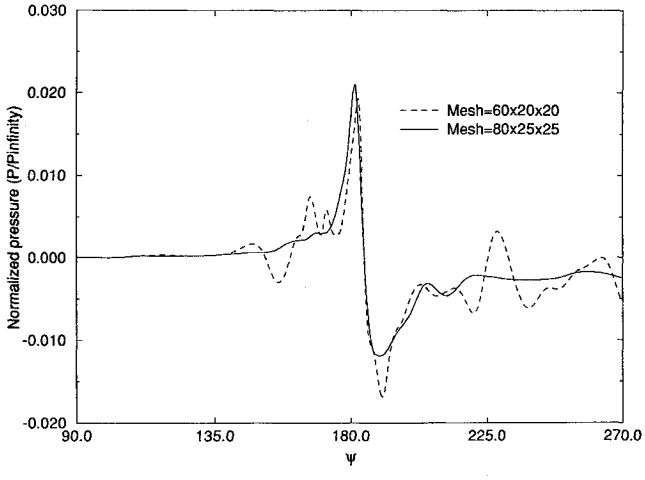

Fig. 8 Different meshes for hover parallel BVI, $M = 0.75$, $\Gamma_v = 0.2$, $Z_v = -0.26$ at a position $x_* = -0.38$, $y_* = 9.89$, $z_* = 0.45$ on control surface $L = 8$.

transform. We were able to show this for the case of a uniformly moving surface.

To examine the rotating Kirchhoff method, a very simple case of a rotating constant point source is used as a test, as shown in Fig. 2. The angular velocity used has the same value as the velocity used later for a hovering rotor speed. The formulation for this simple model is as follows[31]:

$$p(X_*, t_*) = \frac{k}{r(1-M_r)} \tag{18}$$

where r and M_r are defined in Fig. 2 and k is a constant (e.g., k = 1); we used the rotating speed M_s =0.5, R_s =10, and R = 30. For the numerical computation, we applied Farassat's formulation with the control surface S shown in Fig. 1. The computed results are shown in Fig. 3, and these computational results agree with the analytical solution. The mesh used to get this computational result is 60×20, where these are 60 warp-around grid points and 20 spanwise grid points. We can also see from Fig. 3 that increasing the mesh density to 100 × 25 had no significant effect on the computational results. It should be noted that the derivatives based on the analytical calculation are initially used on the rotating Kirchhoff surface. Results from the numerical calculation are also shown in Fig. 3. The differences because of the mesh spacing become larger in this case. Both base surfaces (i.e., top and bottom) are included in the calculations.

Results and Discussion

The numerical analyses were performed on Cray-2 supercomputer. The results shown here are for a nonlifting rotor with the NACA 0012 airfoil section shown in Fig. 1, where aspect ratios of 10 for BVI and HSI were used. The FPR code for an 80 × 25 × 25 mesh with 600 time steps takes about 25 min of CPU time; each time step corresponds to a 0.3-deg rotor azimuth per time step. It should be noted here that to get better results for lift coefficient vs blade rotation ψ, 0.125 deg should be used for $\Delta\psi$. However, the influence of the choice of the $\Delta\psi$ on the far field is small, as will be shown later. The corresponding far-field acoustic code based on the rotating Kirchhoff formula takes less than 2 min of CPU time for one observer position. Since the events that cause the radiated noise are most likely related to events that occur as the rotor rotates (changes azimuth angle ψ), ψ is selected.

The observer's position is defined using distance d and angles α and β shown in Fig. 4. It should be noted that the vortex line is parallel to the Y axis, and the observer is stationary with respect to the undisturbed air, which corresponds to the case of rotor in hover.

Regarding the choice of control surface S, we chose L = 10 as shown in Fig. 1 for most BVI calculations because it seemed to give accurate information on control surface S and it seemed sufficiently large to enclose the most nonlinear effect. However, for HSI noise calculation, we use larger S at L = 14 and the top surface at K = 20, which represents the spanwise position, since the tip Mach number considered was much higher for the cases at M =

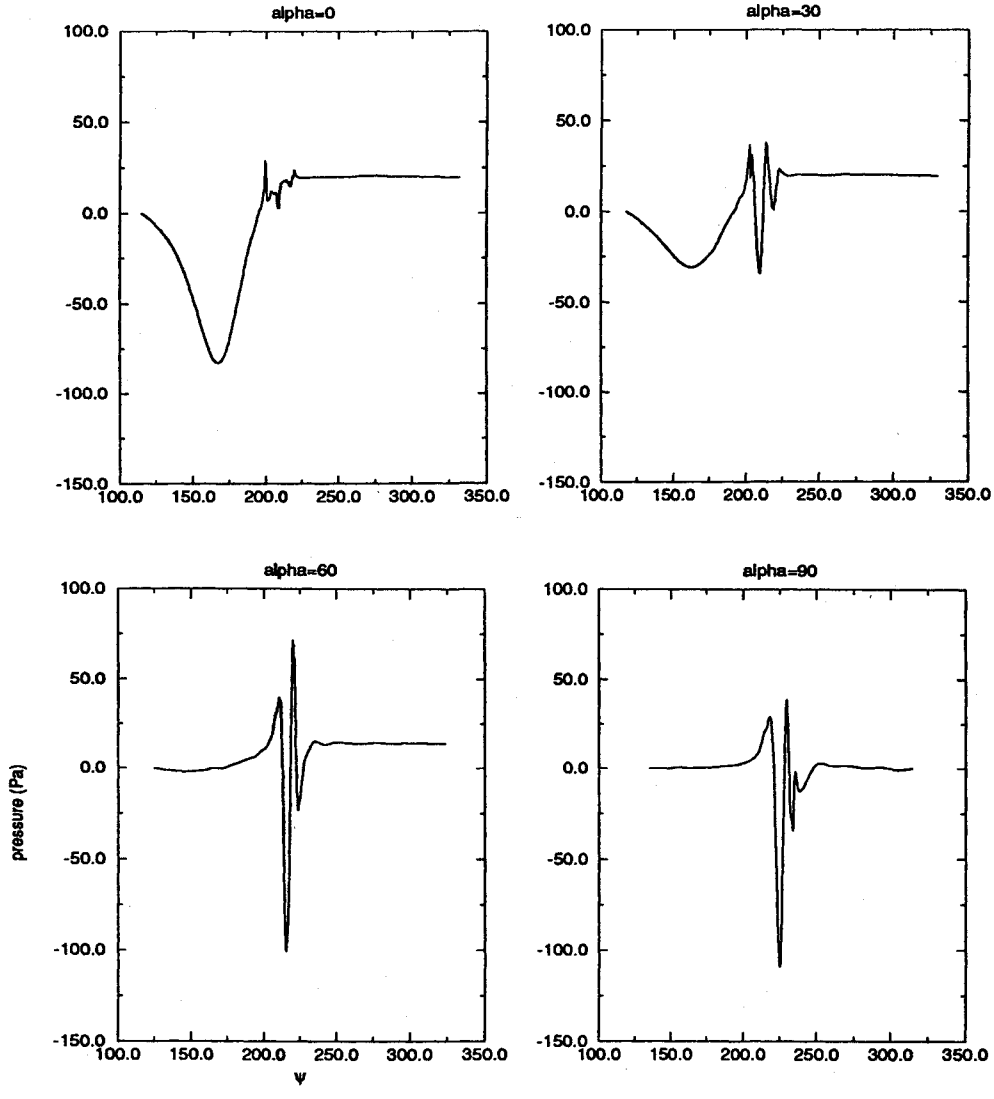

Fig. 9 Noise directivity for hover parallel BVI, M = 0.75, Γ_v = 0.2, Z_v = −0.26 at position d = 3R, β = −30.

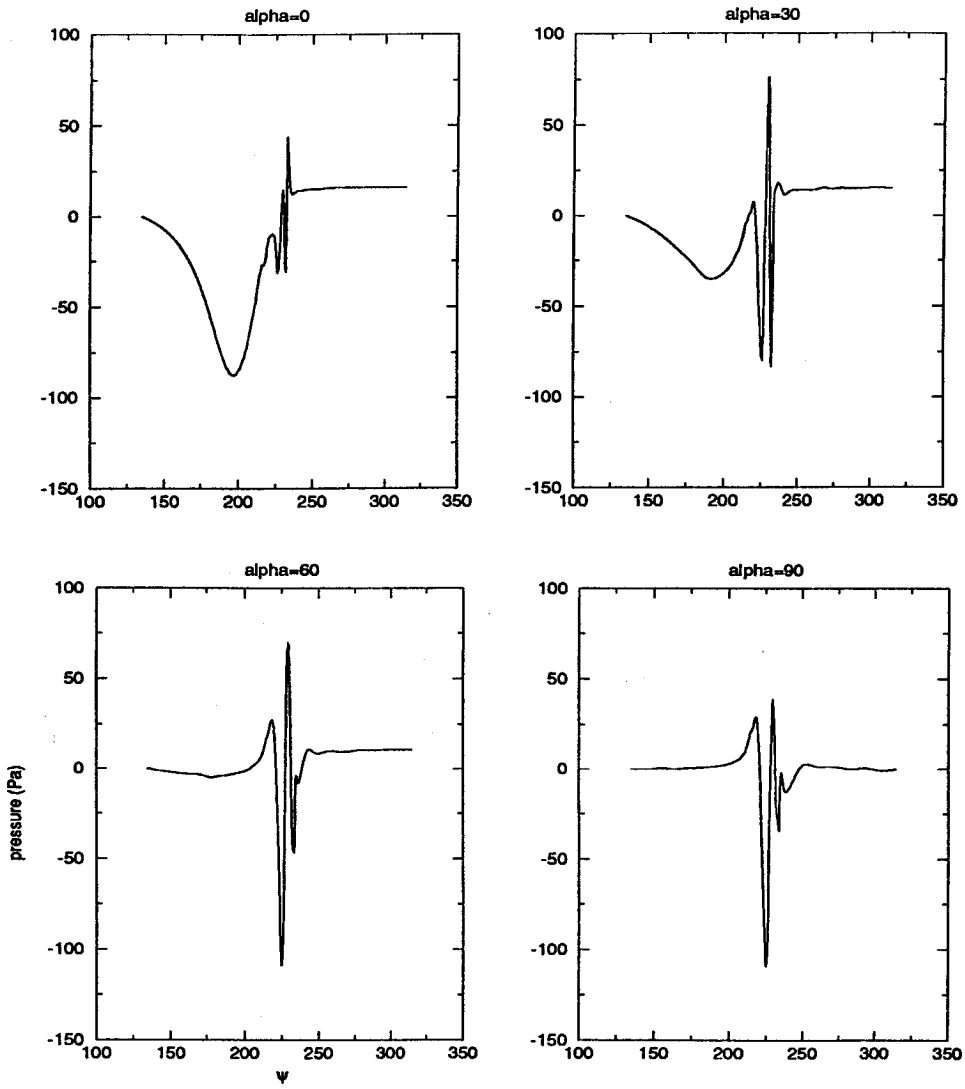

Fig. 10 Noise directivity for hover parallel BVI, $M = 0.75$, $\Gamma_v = 0.2$, $Z_v = -0.26$ at a position $d = 3R$, $\beta = 0$.

0.88 and 0.9. It should also be mentioned here including top surface plays a critical role in capturing HSI noise and, thus, is included in all subsequent calculations.

The main objective of our work is to predict three-dimensional BVI noise. However, our rotating Kirchhoff method is able to predict high-speed impulsive noise too as already mentioned. We calculated the HSI noise, because there are some numerical and experimental results that can be used for comparison (e.g., Purcell[32]). Fig. 5 shows the results of computed far-field pressure (HSI noise); we used similar parameters to Purcell[32] (i.e., 1/7 scale model of a UH-1H rotor). Our results agree well with his numerical and experimental results, as shown in Fig. 5. It should be noted that Purcell[32] used a finer FPR 80 × 50 × 35 grid coupled with a nonlinear Kirchhoff formulation (Isom's formulation[33]). Isom's formulation restricts the position of the stationary Kirchhoff surface on the sonic cylinder and the observer on the rotating plane and high frequencies. The finer mesh was needed to extend the solution to the sonic cylinder. Our rotating Kirchhoff formulation is necessary for the calculation of BVI noise, and it seems that it works very well in computing the HSI noise as well. Our numerical results also compare well with direct CFD calculations using Euler and Navier Stokes calculations,[21] not shown here. Finally, it should be noted that a better FPR mesh might be needed to increase the Mach number beyond 0.9. However, the top base surface can not be extended farther than the sonic cylinder, because the assumption for the Farassat's formula is for subsonic speed motion. The method should be extended to supersonically moving surfaces to address this problem, but it is adequate for tip Mach numbers ≤ 0.95 used herein.

Figure 6 shows the result from Morino's formulation compared to the FPR result. It is for tip Mach number = 0.75, $\Gamma_v = 0.2$, $Z_v = -0.26$ at position on $L = 11$, whereas the control surface is at $L = 10$. It should be noted that the observer's position is moving with the rotating blade, and the distance between them remains fixed. Since it is virtually impossible to measure the signals at the rotating observer's position, the acoustic result from Morino's formula is difficult to compare with experimental data. However, these results can be used to examine the validation of the rotating Kirchhoff method here.

Figure 7 shows the results from Farassat's formula for the previous case with and without BVI in plane noise signals. It appears that the BVI adds two major high-frequency disturbances to the HSI noise signal. For the BVI case, the size of control surfaces S used are $L = 10$ and $K = 21$. The observer's position is shown in the caption.

Figure 8 shows the effect of the mesh on the results. The coarse mesh gives some extra disturbances, whereas the signal for the finer mesh is smoother. Therefore, the finer 80 × 25 × 25 mesh is used in the subsequent calculations.

Figures 9–11 show the noise directivity results from Farassat's formula at various positions. Figure 9 shows the vertical directivity before the vortex line. It should be noted that the second disturbance increases with angle α, showing a similarity to the two-dimensional results.[4] The amplitude variations are caused by the

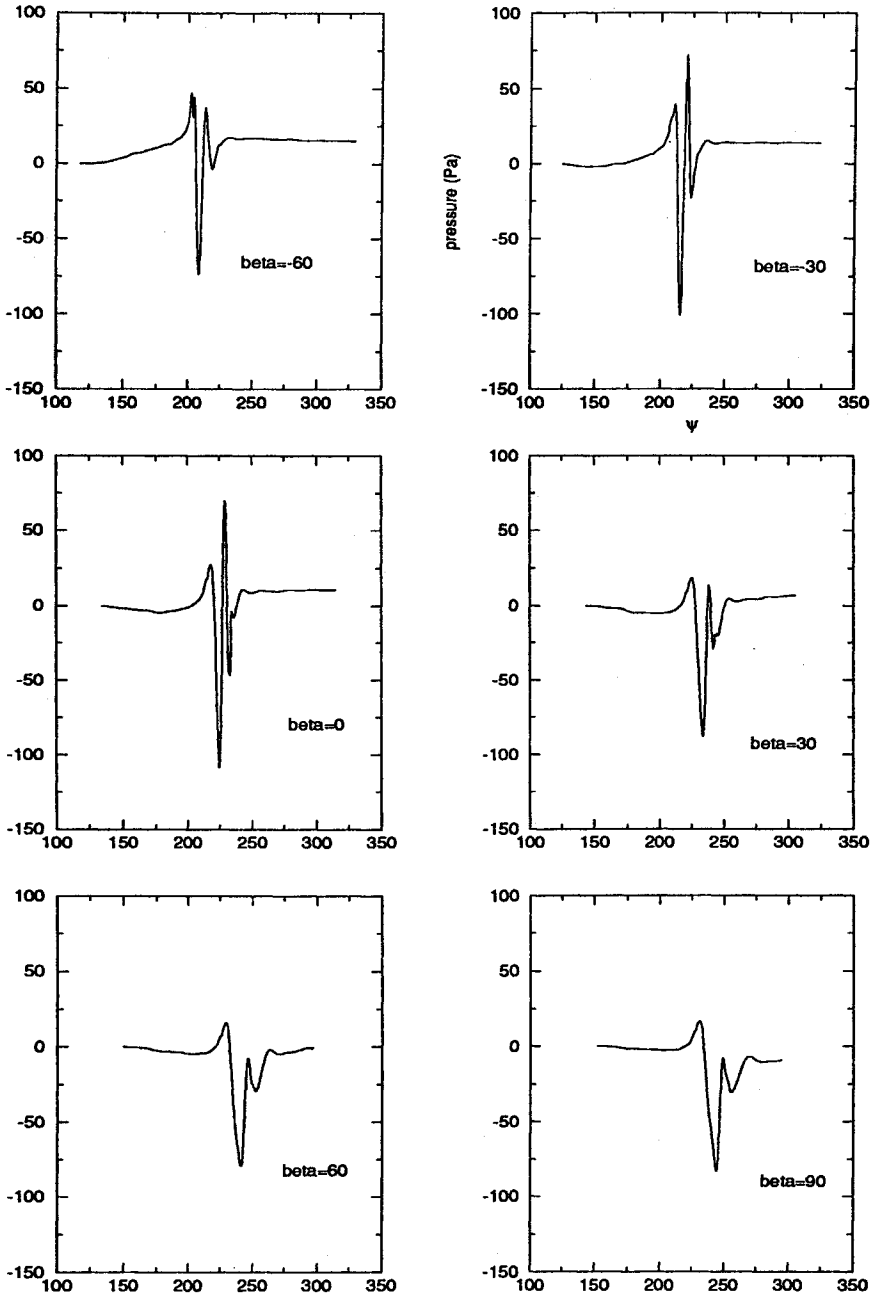

Fig. 11 Noise directivity for hover parallel BVI, $M = 0.75$, $\Gamma_v = 0.2$, $Z_v = -0.26$ at position $d = 3R$, $\alpha = 60$.

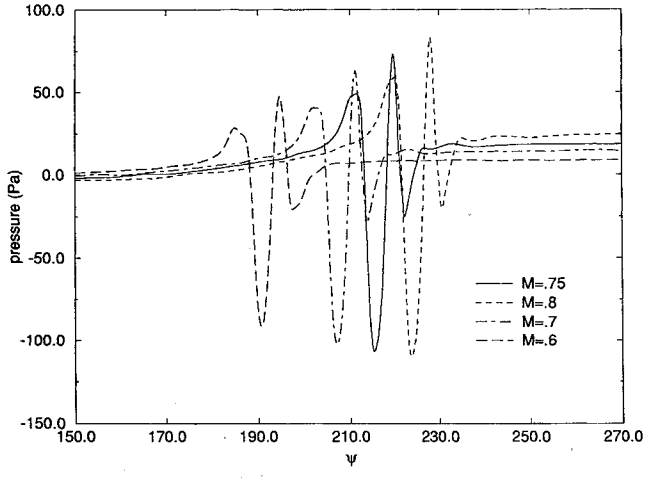

Fig. 12 Different Mach numbers for hover parallel BVI, $M = 0.8$, 0.75, 0.7, and 0.6, $\Gamma_v = 0.2$, $Z_v = -0.26$ at position $d = 3R$, $\alpha = 60$, $\beta = -30$.

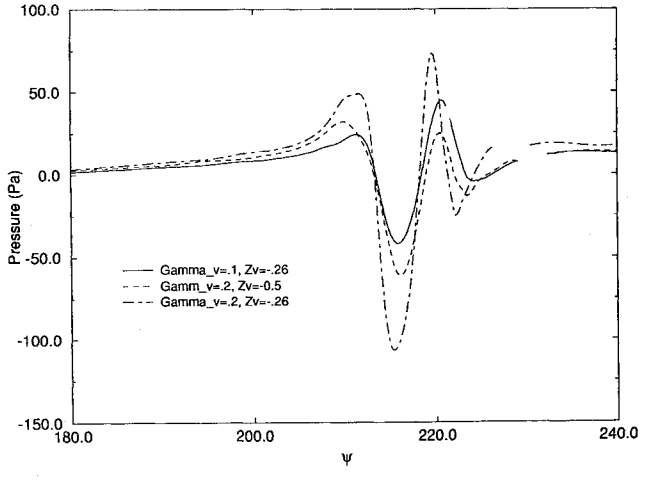

Fig. 13 Different vortex strength and miss distance for hover parallel BVI, $M = 0.75$ at position $d = 3R$, $\alpha = 60$, $\beta = -30$.

different distances between tip blade and observer. The downward directivity of the BVI noise signal is due to the unsteady lift and the unsteady shock wave motion (for the transonic cases) that are induced by the BVI. The HSI noise decreases with increasing α, as expected. The cited phenomena are more clearly shown in Fig. 10, which presents the vertical directivity just under the vortex line. Figure 11 shows the horizontal directivity at $\alpha = 60$, which is the BVI noise dominated region. The stronger signals are observed at the region before the vortex line (i.e., $\beta = -30$). In addition, the BVI noise has a forward directivity on the advancing side before the BVI (i.e., negative β). The signal at the retreating side is mainly due to HSI noise. It should be noted here that some signals at certain positions are longer than the others; that is primarily due to the Doppler frequency shift. The directivity of three-dimensional BVI noise is very complicated (e.g., Ref. 34) and a more detailed investigation is needed.

Figure 12 shows the noise signal for $\alpha = 60$ and $\beta = -30$. We can see that with increasing tip Mach number the two disturbances increase proportionally.

Figure 13 shows the effect of vortex strength and miss distance. Both these parameters have a significant effect in the resulting noise as shown in Fig. 13. A higher vortex strength increases both disturbances. A higher miss distance decreases both disturbances, especially the second one. A low vortex strength and a higher miss distance are desirable for low BVI noise.

Concluding Remarks

A new method has been developed for the computation of the far-field transonic noise due to three-dimensional BVI. A rotating Kirchhoff method is used to calculate the far-field results, with the near-field computed by the FPR code. It shows that this method can predict both far-field BVI and HSI noise, although we have not had the corresponding experimental results for parallel BVI to compare with. The separation of the problem into linear and nonlinear regions allows the use of the most appropriate numerical methodology for each. Two rotating Kirchhoff formulations are presented for this method. They are developed for the hovering rotor case in this paper. However, these rotating Kirchhoff methods can be easily extended to forward flight. This extension is currently sought.

The rotating Kirchhoff method was found to have very good agreement with other experimental and numerical techniques for HSI noise and seemed to be more efficient than other computational methods. This method can also capture both HSI and BVI noise at the same time. It is noted that the three-dimensional noise signals are weaker but more directive in character than two-dimensional results. Important parameters are the tip Mach number, vortex strength, and miss distance. The vortex strength has a more significant effect on the far-field noise. The limited results shown in this paper strengthen our belief that the Kirchhoff method in general is ideal for three-dimensional transonic BVI noise because it can gather all near-field complicated nonlinear effects that are necessary for far-field accurate acoustic prediction. Future stages of the research will extend the formulation for forward flight and supersonically rotating surfaces that are needed for high tip Mach numbers (eg., $M_{tip} > 0.95$). We will also apply it to more complex vortex wake models (i.e., self-generating BVI), e.g., FPR coupled with CAMRAD as in Ref. 35 and more advanced CFD models (e.g., TURNS code).

Acknowledgments

The authors want to thank Roger C. Strawn of the U.S. Aeroflightdynamics Directorate at NASA Ames for providing the FPR code and for his valuable advice toward utilizing it. The calculations were performed at the computational facilities of Minnesota Supercomputer Institute (MSI). This work was also supported by Cray Research, Inc.

References

[1]George, A. R., and Chang, S. B., "Flow Field and Acoustics of Two-dimensional Transonic Blade-Vortex Interactions," AIAA 9th Aeroacoustics Conf., AIAA Paper 84-2309, Williamsburg, VA, Oct. 15–17, 1984.

[2]George, A. R., and Lyrintzis, A. S., "Acoustics of Transonic Blade-Vortex Interactions," *AIAA Journal*, Vol. 26, No. 7, 1988, pp. 769–776.

[3]Lyrintzis, A. S., and George, A. R., "Far-Field Noise of Transonic Blade-Vortex Interactions," *American Helicopter Society Journal*, Vol. 34, No. 3, 1989, pp. 30–39.

[4]Lyrintzis, A. S., and Xue, Y., "A Study of the Noise Mechanisms of Transonic Blade-Vortex Interactions," *AIAA Journal*, Vol. 29, No. 10, 1991, pp. 1562–1572.

[5]McCroskey, W. J., and Goorjian, P. M., "Interactions of Airfoils with Gusts and Concentrated Vortices in Unsteady Transonic Flow," AIAA 16th Fluid and Plasma Dynamics Conf., AIAA Paper 83-1691, Danvers, MA, July 1983.

[6]Srinivasan, G. R., McCroskey, W. J., and Kutler, P., "Numerical Simulation of the Interaction of a Vortex with Stationary Airfoil in Transonic Flow," AIAA Paper 84-0254, Jan. 1984.

[7]Sankar, N. L., and Tang, W., "Numerical Solution of Unsteady Viscous Flow Past Rotor Sections," AIAA Paper 85-0129, Jan. 1985.

[8]Srinivasan, G. R., McCroskey, W. J., and Baeder, J. D., "Aerodynamics of Two-dimensional Blade-Vortex Interaction," *AIAA Journal*, Vol. 24, No. 10, 1986, pp. 1569–1576.

[9]Owen, S. T., and Shenoy, R. K., "Numerical Investigation of Two-Dimensional Blade-Vortex Interaction," *Proceedings of the American Helicopter System National Specialists' Meeting on Aerodynamics and Aeroacoustics*, Arlington, TX, Feb. 1987.

[10]Damodaran, M., and Caughey, D. A., "A Finite Volume Euler Calculation of the Aerodynamics of Transonic Airfoil-Vortex Interaction," *AIAA Journal*, Vol. 26, No. 11, 1988, pp. 1346–1353.

[11]Liu, N.-S., Davoudzadeh, F., Briley, W. R., and Shamroth, S. J., "Navier Stokes Simulation of Transonic Blade-Vortex Interactions," *ASME Journal of Fluids Engineering*, Vol. 112, No. 4, 1990, pp. 501–509.

[12]Lyrintzis, A. S., and Xue, Y., "Acoustics of Transonic Flow Around an Oscillating Flap," *ASME Journal of Fluids Engineering*, Vol. 114, No. 2, 1992, pp. 240–245.

[13]Lyrintzis, A. S., Lee, J., and Xue, Y., "Mechanisms and Directivity of Unsteady Transonic Flow Noise," *ASME Journal of Fluids Engineering* (to be published).

[14]Baeder, J. D., McCroskey, W. J., and Srinivasan, G. R., "Acoustic Propagation Using Computational Fluid Dynamics," *Proceedings of the 42nd Annual Forum of the American Helicopter Society*, Vol. 1, Washington, DC, 1986, pp. 551–562.

[15]Lyrintzis, A. S., and Xue, Y., "A Parametric Study of Transonic Blade-Vortex Interactions," NASA/NAG 2-646 Final Rept., Oct. 1991; also Univ. of Minnesota Supercomputer Inst. Research Rept., UMSI 91/265, Minneapolis, MN, Oct. 1991.

[16]Baeder, J. D., "Euler Solutions to Nonlinear Acoustics of Non-Lifting Rotor Blades," *Proceedings of American Helicopter Society/RAeS International Technical Specialists Meeting on Rotorcraft Acoustics and Rotor Fluid Dynamics* (Philadelphia, PA), 1991.

[17]Brentner, K. S., and Farassat, F., "Helicopter Noise Prediction: The Current Status and Future Direction," *Proceedings of the 14th DGLR/AIAA Aeroacoustics Conference* (Aachen, Germany), AIAA, Washington, DC, 1992, pp. 724–735.

[18]Tadghighi, H., Hassan, A. A., and Charles, B., "Prediction of Blade-Vortex Interaction Noise Using Airloads Generated by a Finite-Difference Technique," *American Helicopter Society Journal*, Vol. 37, No. 4, 1992, pp. 38–47.

[19]Gallman, J. M., "Parametric Computational Study of Isolated Blade-Vortex Interaction Noise," *AIAA Journal*, Vol. 32, No. 2, 1994, pp. 232–238.

[20]Lyrintzis, A. S., "The Use of Kirchhoff Method in Aeroacoustics," *ASME Journal of Fluids Engineering* (to be published).

[21]Baeder, J. D., Gallman, J. M., and Yung, Y., "A Computational Study of the Aeroacoustics of Rotor in Hover," *Proceedings of the 49th Annual Forum of the American Helicopter Society* (St. Louis, MO), Vol. I, American Helicopter Society, 1993, pp. 55–71.

[22]Strawn, R. C., Garceau, M., and Biswas, R., "Unstructured Adaptive Mesh Computations of Rotorcraft High-Speed Impulsive Noise" AIAA Paper 93-4359, Oct. 1993.

[23] Srinivasan, G. R., and Baeder, J. D., "TURNS: A Free-Wake Euler/Navier-Stokes Numerical Method for Helicopter Rotors," *AIAA Journal*, Vol. 31, No. 5, 1993, pp. 959–962.

[24] Srinivasan, G. R., Baeder, J. D., Obayashi, S., and McCroskey, W. J., "Flowfield of a Lifting Rotor in Hover—A Navier-Stokes Simulation," *AIAA Journal*, Vol. 30, No. 10, 1992, pp. 2371–2378.

[25] Xue, Y., and Lyrintzis, A. S., "The Use of Rotating Kirchhoff Formulation for 3-D Transonic BVI Far-field Noise," *Proceedings of the 49th Annual Forum of the American Helicopter Society* (St. Louis, MO), American Helicopter Society, May 1993.

[26]Caradonna, F. X., Strawn, R. C., and Bridgeman, J. O., "An Experimental and Computational Study of Blade-Vortex Interactions," *Vertica*,

Vol. 12, No. 4, 1988, pp. 315–327.

[27]Strawn, R. C., and Caradonna, F. X., "Conservative Full Potential Model for Unsteady Transonic Rotor Flows," *AIAA Journal,* Vol. 25, No. 2, 1987, pp. 193–198.

[28]Morino, L., and Tseng, K., "A General Theory of Unsteady Compressible Potential Flows with Applications to Airplanes and Rotors," *Developments in Boundary Element Methods,* Vol. 6, edited by P. K. Banerjee and L. Morino, Elsevier Applied Science, Barking, England, UK, 1990, pp. 183–245.

[29]Farassat, F., and Myers, M. K., "Extension of Kirchhoff's Formula to Radiation from Moving Surfaces," *Journal of Sound and Vibration,* Vol. 123, No. 3, 1988, pp. 451–461.

[30]Myers, M. K., and Hausmann, J. S., "Computation of Acoustic Scattering from a Moving Rigid Surface," *Journal of the Acoustical Society of America,* Vol. 91, No. 5, 1992, pp. 2594–2605.

[31]Dowling, A. P., and Williams, F., *Sound and Sources of Sound,* Ellis Horwood, England, UK, 1983, pp. 187–192.

[32]Purcell, T. W., "CFD and Transonic Helicopter Sound," 14th European Rotorcraft Forum, Paper No. 2, Milano, Italy, Sept. 1988.

[33] Isom, M., Purcell, T. W., and Strawn, R. C., "Geometrical Acoustics and Transonic Sound," AIAA 11th Aeroacoustics Conf., AIAA Paper 87-2748, Sunnyvale, CA, Oct. 1987.

[34]Ringler, T. D., George, A. R., and Steele, J. B., "A Study of Blade-Vortex Interaction Sound and Directionality," *Proceedings of the American Helicopter Society/RAeS International Technical Specialists Meeting on Rotorcraft Acoustics and Rotor Fluid Dynamics* (Philadelphia, PA), 1991.

[35]Hassan, A. A., Charles, B., Tadghighi, H., and Burley, C., "A Consistent Approach for Modelling the Aerodynamics of Self-Generated Rotor Blade-Vortex Interactions," *Proceedings of the 49th Annual Forum of the American Helicopter Society* (St. Louis, MO), American Helicopter Society, May 1993, pp. 597–615.